

# Multi-Source Video Summarisation

Xiatian Zhu, *Student Member, IEEE*, Chen Change Loy, *Member, IEEE*, and Shaogang Gong

**Abstract**—Many visual surveillance tasks, e.g. video summarisation, is conventionally accomplished through analysing imagery-based features. Relying solely on visual cues for public surveillance video understanding is unreliable, since visual observations obtained from public space CCTV video data are often not sufficiently trustworthy and events of interest can be subtle. On the other hand, non-visual data sources such as weather reports and traffic sensory signals are readily accessible but are not explored jointly to complement visual data for video content analysis and summarisation. In this paper, we present a novel unsupervised framework to learn jointly from both visual and independently-drawn non-visual data sources for discovering meaningful latent structure of surveillance video data. In particular, we investigate ways to cope with discrepant dimension and representation whilst associating these heterogeneous data sources, and derive effective mechanism to tolerate with missing and incomplete data from different sources. We show that the proposed multi-source learning framework not only achieves better video content clustering than state-of-the-art methods, but also is capable of accurately inferring missing non-visual semantics from previously unseen videos. In addition, a comprehensive user study is conducted to validate the quality of video summarisation generated using the proposed multi-source model.

**Index Terms**—Multi-source data, heterogeneous data, visual surveillance, clustering, event recognition, video summarisation.

arXiv:1501.03069v1 [cs.CV] 13 Jan 2015

## 1 INTRODUCTION

VISUAL features and descriptors are often carefully designed and exploited as the sole input for surveillance video content analysis and summarisation. For instance, optical or particle flow is typically employed in activity modelling [1], [2], [3], foreground pixel feature is used for multi-camera video understanding [4], space-time image gradient is adopted for crowd analysis [5], and mixture of dynamic textures is used for video segmentation [6] and anomaly detection [7].

A critical task in visual surveillance is to automatically make sense of massive amount of video data by summarising its content using higher-level intrinsic physical events<sup>1</sup> beyond low-level key-frame visual feature statistics and/or object detection counts. In most contemporary techniques, low-level imagery visual cues are typically exploited as the only information source for video summarisation [8], [9], [10], [11], [12]. On the other hand, in complex and cluttered public scenes there are intrinsically more interesting and salient higher-level events that can provide more meaningful and concise summarisation of the video data. However, such events may not be visually well-defined (easily detectable) nor detected reliably by visual cues alone. In particular, surveillance visual data from public spaces is often inaccurate and/or incomplete due to uncontrollable sources of variation, changes in illumination, occlusion, and background clutters [13].

- Xiatian Zhu and Shaogang Gong are with School of Electronic Engineering and Computer Science, Queen Mary University of London. E-mail: xiatian.zhu@qmul.ac.uk, s.gong@qmul.ac.uk
- Chen Change Loy is with Department of Information Engineering, The Chinese University of Hong Kong. E-mail: ccloy@ie.cuhk.edu.hk

1. Spatiotemporal combinations of human activity or interaction patterns, e.g. gathering, or environmental state changes, e.g. raining.

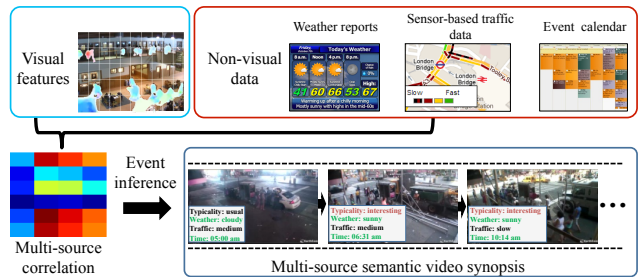


Fig. 1. We consider a novel setting where multiple heterogeneous sources are present during the model training stage. The proposed Constrained Clustering Forest discovers and exploits latent correlations among heterogeneous visual and non-visual data sources both of which can be inaccurate. In deployment, our model uncovers visual content structures and infer semantic tags on previously unseen video data for video summarisation.

In the context of video surveillance, there are a number of non-visual auxiliary information that can be used to complement the unilateral perspective from visual observations. Examples of non-visual sources include weather report, GPS-based traffic data, geo-location data, textual data from social networks, and on-line event schedules. This is because despite that visual and non-visual data may have very different characteristics and are of different natures, they depict the common physical phenomenon in a scene. They are intrinsically correlated, although may be mostly indirect in some latent spaces. Effectively discovering and exploiting such a latent correlation space can facilitate the underlying data structure discovery and bridge the semantic gap between low-level visual features and high-level semantical interpretation.

Nevertheless, unsupervised mining of latent correlation and interaction between heterogeneous data sources faces a number of challenges due to: (1) Disparate sources significantly differ in representation (continuous or categorical),

and largely vary in scale and covariance<sup>2</sup>. In addition, the dimension of visual sources often exceeds that of non-visual information to a great extent ( $>2000$  visual dimensions vs.  $<10$  non-visual dimensions). Owing to this dimensionality discrepancy problem, a straightforward concatenation of features will result in a representation unfavourably inclined towards the imagery data. (2) Both visual and non-visual data in isolation can be inaccurate and incomplete, especially in surveillance data from public spaces. (3) Non-visual information, e.g. event time tables, may not be necessarily available all the time that correspond to visual observations, and vice versa. This renders models that expect full and complete input representation impractical. No existing methods are readily applicable to address all the aforementioned challenges in a unified framework.

The objective of this study is to investigate the joint learning problem given heterogeneous multi-sources. Specifically, we aim to learn an unsupervised model that associates both visual (e.g. optical flow at distributed physical locations) and non-visual (e.g. physical events) data for discovering the underlying video data structure (Fig. 1). The learned model can then be used for surveillance video clustering and event inference on previously unseen data. To illustrate the usefulness of our model, we address this multi-source learning problem in the context of video summarisation, conventionally based on visual feature analysis and object detection/segmentation. Here, we wish to study the complementary role of non-visual auxiliary information in offering a more complete and holistic understanding of a visual scene.

The main contributions of this work are: (1) We propose a unified multi-source learning framework capable of discovering semantic structures of video content collectively from heterogeneous visual and non-visual data. This is made possible by formulating a novel Constrained Clustering Forest (CC-Forest) that seamlessly handles multi-heterogeneous data sources dissimilar in representation, distribution, and dimension. Specifically, our model’s objective function naturally incorporates low-dimensional non-visual data as constraints over high-dimensional visual data. Although both visual and non-visual data in isolation can be inaccurate and incomplete, our model is capable of uncovering and subsequently exploiting the shared latent correlation for better data structure discovery. (2) The model is novel in its ability to accommodate partial or completely missing non-visual sources. In particular, we introduce a joint information gain function that is capable of dynamically adapting to arbitrary amount of missing non-visual constraints during model learning. In model deployment, only visual input is required for inferring missing non-visual semantics, relaxing the need for intensive non-visual data collection. (3) We show that the additional non-visual constraint encourages more balanced and shallower decision trees than learning from single visual source alone. This leads to not only superior model training and inference efficiency, but also improved clustering performance.

Extensive comparative evaluations are conducted on two public surveillance videos captured from both indoor and outdoor environments. Comparative results show that the proposed model not only outperforms standard  $k$ -means and the state-of-the-art methods [15], [16] for video content clustering and structure discovery, but also is more superior in predicting non-visual tags for previously unseen videos. The robustness of the proposed model is further validated by a user study on video synopsis (or summary)<sup>3</sup> quality.

## 2 RELATED WORK

**Multi-modality learning** - There exist studies that exploit different sensory or information modalities from a single source for data structure mining. For example, Cai et al. [17] propose to perform multi-modal image clustering by learning a commonly shared graph-Laplacian matrix from different visual feature modalities. Heer and Chi [18] combine linearly individual similarity matrices derived from multi-modal webpages for web user grouping. Karydis et al. [19] present a tensor based model to cluster music items with additional tags. In terms of video analysis, the auditory channel and/or transcripts have been widely explored for detecting semantic concepts from multimedia videos [20], [21], summarising highlights in news and broadcast programs [22], [23], or locating speakers [24]. User tags associated with web videos (e.g. YouTube) have also been utilised [25], [26], [27]. In contrast, surveillance videos captured from public spaces are typically without auditory signals nor any synchronised transcripts and user tags available. Instead, we wish to explore alternative non-visual data drawn independently elsewhere from multiple sources, with inherent challenges of being inaccurate and incomplete, unsynchronised to and may also be in conflict with the observed visual data.

**Multi-source learning** - An alternative multi-source learning mechanism can be clustering ensemble [28], [29] where a collection of clustering instances is generated and then aggregated into the final clustering solution. Typically only single data source is considered, but it can be easily extended to handle multi-source data, e.g. creating a respective clustering instance for each source. Nonetheless, cross-source correlation is ignored since the clustering instances are separately formed and no interaction between them is involved. A closer approach to ours is the Affinity Aggregation Spectral Clustering (AASC) [15], which learns data structure from multiple types of homogeneous information (visual features only). Their method generates independently multiple affinity data matrices by exhaustive pairwise distance computation for every pair of samples in every data source. It suffers from unwieldy representation given high-dimensional data inputs. Importantly, despite that it seeks for optimal weighted combination of distinct affinity matrices, it does not consider correlation between different sources in model learning, similar to clustering ensemble [28], [29]. Differing from the above models,

2. Also known as the heteroscedasticity problem [14].

3. We use ‘synopsis’ and ‘summary’ interchangeably in this study.

our constrained clustering forest overcomes these problems by generating a unified single affinity matrix that captures latent correlations among heterogeneous types of data sources. Furthermore, our model has a unique advantage in handling missing non-visual data over [28], [29], [15].

**Video summarisation** - Contemporary video summarisation methods can be broadly classified into two paradigms, key-frame-based [11], [30], [31], [32], [33] and object-based [9], [10], [34] methods. The key-frame-based approaches select representative key-frames by analysing low-level imagery properties, e.g. optical flow [30] or image differences [31], object’s appearance and motion [11], to form a storyboard of still images. Object-based techniques [9], [10], on the other hand, rely on object segmentation and tracking to extract object-centric trajectories/tubes, and compress those tubes to reduce spatiotemporal redundancy.

Both the above schemes utilise solely visual information and make implicit assumptions about the completeness and accuracy of the visual data available in extracting features or object-centered representations. They are unsuitable nor scalable to complex scenes where visual data are inherently incomplete and inaccurate, mostly the case in surveillance videos. Our work differs significantly to these studies in that we exploit not only visual data without object tracking, but also non-visual sources as complementary information. The synopsis generated by our approach is semantically enriched – it is labelled automatically with semantic tags, e.g. traffic condition, weather, or event. All these tags are learned from heterogeneous non-visual sources in an unsupervised manner during model training without any manual labels.

**Random forests** - Random forests [35], [16] have proven as powerful models in the literature. Different variants of random forests have been devised, either supervised [36], [37], [38], [39], [40], or unsupervised [41], [42], [43], [44], [45], [46]. Supervised models are not suitable to our problem since we do not assume the availability of ground truth labels during model training. Existing clustering forest models, on the other hand, assumes only homogeneous data sources such as pure imagery-based features. No principled way of combining multiple heterogeneous and independent data sources in forest models is available.

### 3 MULTI-SOURCE VIDEO CLUSTERING

Video summarisation by content abstraction aims to generate a compact summary composed of key/interesting content from a long unseen video for achieving efficient holistic understanding [32]. A common way to establish a summary is by extracting and then combining a set of key frames or shots. These key contents are usually discovered and selected from clusters of video frames or shots [32].

In this study, we follow the aforementioned approach but consider not only visual content of video, but also a large corpus of non-visual data collected from heterogeneous independent sources (Fig. 2(a)). Specifically, through learning latent structure of multi-source data (Fig. 2(b-c)), we wish to make reference to and/or impose non-visual semantics

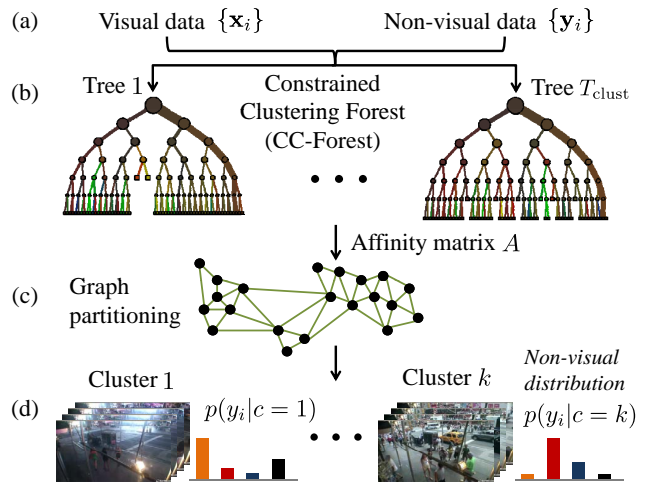


Fig. 2. The pipeline of clustering video data with CC-Forest.

directly into video content clustering without any human manual annotation of video data (Fig. 2(d)). Once such a latent semantic video clustering model is learned from some training data, it is then deployed for semantic video summarisation together with automatic tagging of previous unseen video data by model inference.

Formally, we consider the following different data sources that form a multi-source input feature space:

**Visual features** - We segment a training video into  $N$  either overlapping or non-overlapping clips, each of which has a duration of  $T_{\text{clip}}$  seconds. We then extract a  $d$ -dimensional visual descriptor from the  $i$ th clip denoted by  $\mathbf{x}_i = (x_{i,1}, \dots, x_{i,d}) \in \mathbb{R}^d, i = 1, \dots, N$ .

**Non-visual data** - Non-visual data are collected from heterogeneous independent sources. We collectively represent  $m$  types of non-visual data associated with the  $i$ th clip as  $\mathbf{y}_i = (y_{i,1}, \dots, y_{i,m}) \in \mathbb{R}^m, i = 1, \dots, N$ . Note that any (or all) dimension of  $\mathbf{y}_i$  may be missing.

We need to formulate a model to cope with the few challenges highlighted in Section 1. The model needs to be unsupervised since no ground truth is assumed. To mitigate the heteroscedasticity and dimension discrepancy problems, we need a model that can isolate the very different characteristics of visual and non-visual data, yet can still exploit their latent correlation in the clustering process. To handle noisy data, feature selection is needed.

In light of the above needs, we choose to start with the clustering random forest [35], [41], [42] due to (1) unsupervised information gain optimisation thus requiring no ground truth labels; (2) its flexible objective function for facilitating the modelling of multi-source data as well as the processing of missing data; (3) its implicit feature selection mechanism for handling noisy features. Nevertheless, the conventional clustering forest is not well suited to solve our problem since it expects a full concatenated representation as input during both model training and deployment. This does not conform to the assumption of only visual data being available during model deployment for unseen videos. Moreover, due to its uniform variable selection mechanism [35], there is no principled way to

ensure equal contribution from individual visual and non-visual sources in the node splitting process. To overcome these limitations, we develop a new *Constrained Clustering Forest (CC-Forest)* by introducing a new objective function allowing *joint optimisation of individual information gains* of different sources. We first describe the conventional forests before detailing the proposed CC-Forest.

### 3.1 Conventional Random Forests

**Classification forests** - A general form of random forests is the classification forests. A classification forest [35], [47] is an ensemble of  $T_{\text{class}}$  binary decision trees  $\mathcal{T}(\mathbf{x})$ :  $\mathcal{X} \rightarrow \mathbb{R}^K$ , with  $\mathcal{X}$  the  $d$ -dimensional feature space, and  $\mathbb{R}^K = [0, 1]^K$  denoting the space of class probability distribution over the label space  $\mathcal{L} = \{1, \dots, K\}$ .

Decision trees are learned independently from each other, each with a random subset  $\mathbf{X}_t$  of the training samples  $\mathbf{X} = \{\mathbf{x}_i\}$ , i.e. bagging [35]. Growing a decision tree involves a recursive node splitting procedure until some stopping criterion is satisfied, e.g. leaf nodes are formed when no further split can be achieved given the objective function, or the number of training samples arriving at a node is smaller than the predefined node size,  $\phi$ . Small  $\phi$  leads to deep trees. We set  $\phi = 2$  in our experiments for capturing sufficiently fine-grained data structure. At each leaf node, the class probability distribution is then estimated based on the labels of the arrival samples.

The training of each internal/split node is a process of binary split function optimisation, defined as

$$h(\mathbf{x}, \vartheta) = \begin{cases} 0 & \text{if } x_{\vartheta_1} < \vartheta_2, \\ 1 & \text{otherwise.} \end{cases} \quad (1)$$

This split function is parameterised by two parameters  $\vartheta = (\vartheta_1, \vartheta_2)$ : (i) a feature dimension  $x_{\vartheta_1}$  with  $\vartheta_1 \in \{1, \dots, d\}$ , and (ii) a feature threshold  $\vartheta_2 \in \mathbb{R}$ . All samples of a split node  $s$  will be channelled to either the left  $l$  or right  $r$  child nodes, according to the output of Eqn. (1).

The optimal split parameter  $\vartheta^*$  is chosen via

$$\vartheta^* = \underset{\Theta}{\operatorname{argmax}} \Delta \mathcal{I}_{\text{class}}, \quad (2)$$

where  $\Theta = \{\vartheta^i\}_{i=1}^{m_{\text{try}}(|S|-1)}$  represents a parameter set over  $m_{\text{try}}$  randomly selected features, with  $S$  the sample set reaching the node  $s$ . The cardinality of a set is given by  $|\cdot|$ . Typically, a greedy search strategy is exploited to identify  $\vartheta^*$ . The information gain  $\Delta \mathcal{I}_{\text{class}}$  is formulated as

$$\Delta \mathcal{I}_{\text{class}} = \mathcal{I}_s - \frac{|L|}{|S|} \mathcal{I}_l - \frac{|R|}{|S|} \mathcal{I}_r, \quad (3)$$

where  $L$  and  $R$  denote the sets of data routed into  $l$  and  $r$ , and  $L \cup R = S$ . The information gain  $\mathcal{I}$  can be computed as either the entropy or Gini impurity [48].

**Clustering forests** - In contrast to classification forests, clustering forests require no ground truth label information during the training phase. A clustering forest consists of  $T_{\text{clust}}$  binary decision trees. The leaf nodes in each tree define a spatial partitioning of the training data. Interestingly, the training of a clustering forest can be performed

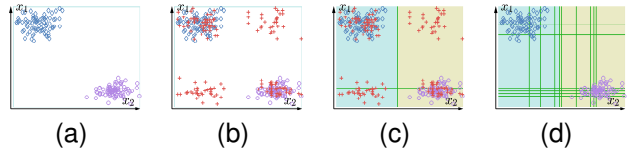


Fig. 3. An illustration of clustering toy data with forest. (a) Original toy data are labelled as class 1, whilst (b) the pseudo-points as class 2. (c) A clustering forest performs two-class classification in the augmented space. (d) The final data partitions in the original data.

using the classification forest optimisation approach by adopting the pseudo two-class algorithm [35], [41], [42]. Specifically, we add  $N$  pseudo samples  $\bar{\mathbf{x}} = \{\bar{x}_1, \dots, \bar{x}_d\}$  (Fig. 3(b)) into the original data space  $\mathbf{X}$  (Fig. 3(a)), with  $\bar{x}_i \sim \text{Dist}(x_i)$  sampled from certain distribution  $\text{Dist}(x_i)$ . In the proposed model, we adopt the empirical marginal distributions of the feature variables owing to its favourable performance [42]. With this data augmentation strategy, the clustering problem becomes a canonical classification problem that can be solved by the classification forest training method as discussed above. The key idea behind this algorithm is to partition the augmented data space into dense and sparse regions (Fig. 3(c-d)) [41].

### 3.2 Multi-Source Constrained Clustering Forest

The *main difference* of our CC-Forest with respect to the conventional clustering forests is that instead of taking a forcefully concatenated visual + non-visual vector as model input, it exploits the non-visual information as *constraints* over visual data to guide the tree formation, whilst still using visual features as splitting-variables to grow constrained clustering trees (CC-trees). Formally, we define a new joint information gain function for node splitting as:

$$\Delta \mathcal{I} = \underbrace{\alpha_v \frac{\Delta \mathcal{I}_v}{\mathcal{I}_{v0}}}_{\text{visual}} + \underbrace{\sum_{j=1}^m \alpha_j \frac{\Delta \mathcal{I}_j}{\mathcal{I}_{j0}}}_{\text{non-visual}} + \underbrace{\alpha_t \frac{\Delta \mathcal{I}_t}{\mathcal{I}_{t0}}}_{\text{temporal}}, \quad (4)$$

whilst the terms in Eqn. (4) are:

**Visual term:**  $\Delta \mathcal{I}_v = \Delta \mathcal{I}_{\text{class}}$  (Eqn. (3)) denotes the information gain in visual domain. In this study we utilise the Gini impurity  $\mathcal{G}$  [48] to estimate  $\Delta \mathcal{I}_{\text{class}}$  by setting  $\mathcal{I} = \mathcal{G}$  in Eqn. (3) due to its simplicity and efficiency. The Gini impurity is computed as  $\mathcal{G} = \sum_{i \neq j} p_i p_j$  with  $p_i$  and  $p_j$  being the proportion of samples belonging to the  $i$ th and  $j$ th category in a split node  $s$ . High value in  $\mathcal{G}$  indicates pure category distribution.

**Non-visual term:** This is a new term we introduce as constraints on visual term. Non-visual data are regarded as *constraints* since we only utilise visual features as splitting variables whilst the selection criterion of the optimal visual data split additionally takes into account non-visual sources as extra enforced conditions.

More specifically,  $\Delta \mathcal{I}_j$  denotes the information gain in the  $j$ th non-visual data. A non-visual source can be either categorical or continuous. For a categorical non-visual source, similar to visual term we use the Gini impurity  $\mathcal{G}$  as its data split measure criterion. In the case of non-visual

source with continuous values, we adopt least squares regression [48] to enforce continuity in the clustering space:

$$\mathcal{R} = \frac{1}{|S|} \sum_{i=1}^{|S|} (y_{i,j} - \frac{1}{|S|} \sum_{i=1}^{|S|} y_{i,j})^2, \quad (5)$$

where  $y_{i,j}$  represents the feature value in the  $j$ th non-visual space associated with the  $i$ th sample  $\mathbf{x}_i \in S$ , and  $S$  is the set of samples reaching node  $s$ . That is  $\Delta\mathcal{I}_j = \mathcal{R}$ . In this way, the joint information gain of visual and non-visual information encourages data separation not only in the visual domain, but also in the auxiliary non-visual constraint domains.

**Temporal term:** We also add a temporal smoothness gain  $\Delta\mathcal{I}_t$  to encourage temporally adjacent video clips to be grouped together. This temporal constraint helps in mining visual data structure.

The information gain by different sources may live in very disparate ranges due to the different natures of source, each term of Eqn. (4) is therefore normalised by its initial data impurity denoted by  $\mathcal{I}_{v0}$ ,  $\mathcal{I}_{j0}$ , and  $\mathcal{I}_{t0}$ . These impurities are obtained at the root node of every CC-tree.

The source weights are denoted by  $\alpha_v$ ,  $\alpha_i$ , and  $\alpha_t$  accordingly, holding  $\alpha_v + \sum_{i=1}^m \alpha_i + \alpha_t = 1$ . We set  $\alpha_v = 0.5$  obtained by cross-validation. A detailed analysis on  $\alpha_v$  is given in Section 6.2. For non-visual and temporal constraints, we uniformly assign  $\alpha_t = \alpha_i = \frac{1-\alpha_v}{m+1}$  since their importance is not known *in prior*, with  $m$  the number of non-visual sources.

The above formulation brings two unique benefits: (I) Thanks to the information gain optimisation, the influences of visual and non-visual domains on data partitioning can be better balanced compared to naïve feature concatenation. (II) Eqn. (2) and Eqn. (4) together provide a mechanism to discover strongly correlated heterogeneous source pairs and exploit joint information gain of such correlated pairs for data partitioning. In other words, only selective visual features (Eqn. (2)) that yield high information gain collectively with non-visual constraints (Eqn. (4)) will contribute to the tree growing. Such a mechanism cannot be realised using the conventional clustering forests [35], [41].

### 3.2.1 Coping with Partial/Missing Non-Visual Data

We introduce a new adaptive weighting mechanism to dynamically deal with the inevitable partial/missing non-visual data. Specifically, when some non-visual data are missing and suppose the missing proportion of the  $i$ th non-visual type in the training set  $\mathbf{X}_t$  for CC-tree  $t$  is  $\delta_i$ , we reduce its weight from  $\alpha_i$  to  $\alpha_i - \delta_i \alpha_i$ . The total reduced weight  $\sum_i \delta_i \alpha_i$  is then distributed evenly to the weights of all sources to ensure  $\alpha_v + \sum_{i=1}^m \alpha_i + \alpha_t = 1$ . This linear adaptive weighting method produces satisfactory results in our experiments.

### 3.2.2 Quantifying Correlation between Sources

Quantifying latent correlation between different sources gives insights into their interactions in forming coherent video groupings. This can be done once a CC-Forest is

trained. To quantify between-source correlation, we first estimate correlation among their constituent features.

**Visual-visual feature correlation** - Visual-visual feature correlation is typically quantified based on their similarity in inducing split node partitions  $L$  and  $R$  [35]. In particular, given a split node  $s$  and its final optimal split, say  $L_\nu$  and  $R_\nu$  by feature  $\nu$ . From Eqn. (2), we recall that this feature  $\nu$  is selected out from the  $m_{\text{try}}$  randomly sampled features  $F^s = \{f_1, \dots, f_{m_{\text{try}}}\}$ . Let  $\tau \in F^s \setminus \nu$  and its optimal left-right partitions be  $L_\tau$  and  $R_\tau$  respectively. The node-level correlation between features  $\nu$  and  $\tau$  is then defined as

$$\lambda_f(\nu, \tau) = \frac{p_\nu - (1 - \frac{|L_\nu \cap L_\tau|}{|L_\nu \cup R_\nu|} - \frac{|R_\nu \cap R_\tau|}{|L_\nu \cup R_\nu|})}{p_\nu}, \quad (6)$$

where  $p_\nu = \min(\frac{|L_\nu|}{|L_\nu|+|R_\nu|}, \frac{|R_\nu|}{|L_\nu|+|R_\nu|})$ , thus  $p_\nu \in (0, \frac{1}{2}]$ . With Eqn. (6) we assign a strong correlation ( $\lambda_f(\nu, \tau) = 1$ ) to a feature pair  $(\nu, \tau)$  if they produce the same data partition, whilst a weak correlation ( $\lambda_f(\nu, \tau) \leq -1$ ) when their partitions have no overlaps. For simplicity we let  $\lambda_f(\nu, \tau) = \max(\lambda_f(\nu, \tau), 0)$  such that  $\lambda_f(\nu, \tau)$  lies in the range of  $[0, 1]$ . The final visual-visual feature correlation  $\lambda(\nu, \tau)$  is obtained via

$$\lambda(\nu, \tau) = \frac{1}{T_{\text{clust}}} \sum_{t=1}^{T_{\text{clust}}} \left[ \frac{1}{N_{(\nu, \tau)}^t} \sum_k^{N_{(\nu, \tau)}^t} \lambda_f(\nu, \tau) \right], \quad (7)$$

where  $N_{(\nu, \tau)}^t$  refers to the number of sampling co-occurrences of a feature pair  $(\nu, \tau)$  during the splitting process of a CC-tree  $t$ .

**Visual-nonvisual feature correlation** - Recall that visual and non-visual data play different roles in our CC-Forest, e.g. the former as splitting features whereas the later as constraints. This difference makes the above equations not applicable to the computation of visual-nonvisual feature correlation since no data split is associated with non-visual features. Instead, we adopt information gain as the visual-nonvisual feature correlation metric. This metric is appropriate in that it also reflects the intrinsic mutual interaction between visual and non-visual features during joint information gain optimisation (Eqn. (4)). Formally, we quantify the node-level correlation between the optimal splitting visual feature  $\nu$  and a non-visual feature  $\omega$  as  $\lambda_f(\nu, \omega) = \frac{\Delta\mathcal{I}_\omega}{\mathcal{I}_{\omega 0}}$  (the non-visual term of Eqn. (4)). The final visual-nonvisual feature correlation  $\lambda(\nu, \omega)$  is computed similarly by Eqn. (7).

**Correlation between sources** - Given between-feature correlation, the final correlation between any two sources  $\xi_i$  and  $\xi_j$  can then be estimated through

$$\psi(\xi_i, \xi_j) = \frac{1}{|\xi_i||\xi_j|} \sum_{\nu \in \xi_i, \tau \in \xi_j} \lambda(\nu, \tau). \quad (8)$$

### 3.2.3 Model Complexity

The upper-bound learning complexity of a whole CC-Forest can be examined from its constituent parts, i.e. at tree- and node-levels. Formally, given a CC-tree  $t$ , we denote the set of all the split nodes as  $\Pi_t$  and the sample subset

used for training a split node  $j \in \Pi_t$  as  $S_j$ . The training complexity of  $j$ -th node is given by  $m_{\text{try}}(|S_j|-1)u$ , when a greedy search algorithm is adopted, with  $m_{\text{try}}$  the number of features attempted to partition  $S_j$ , and  $u$  the running time of conducting one data splitting operation. Consequently, the overall computational cost of learning a CC-Forest can be computed as

$$\Omega = \sum_t^{T_{\text{clust}}} \sum_{j \in \Pi_t} m_{\text{try}}(|S_j|-1)u = m_{\text{try}}u \sum_t^{T_{\text{clust}}} \sum_{j \in \Pi_t} (|S_j|-1). \quad (9)$$

The value of parameter  $m_{\text{try}}$  is identical across all CC-trees. The learning time is thus determined by (1) the value of  $u$ , and (2) the factor that we name as *tree fan-in*

$$\Phi(t) = \sum_{j \in \Pi_t} |S_j - 1|. \quad (10)$$

Clearly,  $u$  of a CC-Forest is larger than that of conventional forests since we need to compute additional information gains of non-visual and temporal constraints (Eqn. (4)). On the other hand, the value of  $\Phi(t)$  primarily relies on the tree structure/topological characteristics [49]: a balanced and shallower tree has smaller  $\Phi(t)$ , thus the tree shall be more efficient in training and inference on unseen samples, in that the paths from the root to leaf nodes are relatively shorter. In Section 6.4, we will show that the additional non-visual constraint encourages more balanced and shallower decision trees than learning from single visual source alone.

### 3.3 Latent Data Structure Discovery

The multi-source feature space has high dimension (over 2000 dimensions). This makes learning data structure by clustering computationally difficult. To this end, we consider spectral clustering on manifold to discover latent clusters in a lower dimensional space. Fig. 2 depicts the pipeline of our video data clustering approach based on the learned CC-Forest.

Spectral clustering [50] groups data using eigenvectors of an affinity matrix derived from the data. The learned CC-Forest offers an effective way to derive the required affinity matrix. Specifically, each individual tree within the CC-Forest partitions the training samples at its leaves  $\ell(\mathbf{x})$ :  $\mathbb{R}^d \rightarrow \mathbf{L} \subset \mathcal{N}$ , where  $\ell$  represents a leaf index and  $\mathbf{L}$  refers to the set of all leaves in a given tree. For each CC-tree, we first compute a tree-level  $N \times N$  affinity matrix  $A^t$  with elements defined as  $A_{i,j}^t = \exp^{-\text{dist}(\mathbf{x}_i, \mathbf{x}_j)}$  where

$$\text{dist}(\mathbf{x}_i, \mathbf{x}_j) = \begin{cases} 0 & \text{if } \ell(\mathbf{x}_i) = \ell(\mathbf{x}_j), \\ +\infty & \text{otherwise.} \end{cases} \quad (11)$$

We assign the maximum affinity (affinity=1, distance=0) between points  $\mathbf{x}_i$  and  $\mathbf{x}_j$  if they fall into the same leaf, and the minimum affinity (affinity=0, distance=1) otherwise. A smooth affinity matrix can be obtained through averaging all the tree-level affinity matrices

$$A = \frac{1}{T_{\text{clust}}} \sum_{t=1}^{T_{\text{clust}}} A^t, \quad (12)$$

Equation (12) is adopted as the ensemble model of CC-Forest due to its advantage of suppressing the noisy tree predictions, though other alternatives such as the product of tree-level predictions are possible [16]. We then construct a sparse  $k$ -NN graph, whose edge weights are defined by  $A$  (Fig. 2(c)).

Subsequently, we symmetrically normalise  $A$  to obtain  $S = D^{-\frac{1}{2}}AD^{-\frac{1}{2}}$ , where  $D$  denotes a diagonal degree matrix with elements  $D_{i,i} = \sum_j^N A_{i,j}$ . Given  $S$ , we perform spectral clustering to discover the latent clusters of training clips with the number of clusters automatically determined through analysing the eigenvector structure [50]. Each training clip  $\mathbf{x}_i$  is then assigned to a cluster  $c_i \in \mathcal{C}$ , with  $\mathcal{C}$  the set of all clusters.

The learned clusters group similar clips both visually and semantically, with each of the clusters associated with a unique distribution for each non-visual data (Fig. 2-d). We denote the distribution of the  $i$ th non-visual data type of the cluster  $c$  as

$$p(y_i|c) \propto \sum_{\mathbf{x}_j \in \mathbf{X}_c} p(y_i|\mathbf{x}_j), \quad (13)$$

where  $\mathbf{X}_c$  represents the set of training samples in  $c$ .

## 4 MULTI-SOURCE VIDEO SUMMARISATION

In Section 3 we presented multi-source clustering by learning a Constrained Clustering Forest (CC-Forest). Once the CC-Forest is learned, it can be deployed for semantic video summarisation. Specifically, we follow the established approach of summarising videos by clustering [32] but with the introduction of two noticeable differences in our method.

First, our *video summary is multi-source referenced*. Specifically, the CC-Forest is trained on heterogeneous sources, its optimised split functions  $\{h\}$  (Eqn. (1)) therefore implicitly capture the complex multi-source structures. When one deploys the trained model for content summarisation of previously unseen video data, the model only needs to take visual inputs without any non-visual data sources. And yet it is able to induce video content partitions that not only correspond to visual feature similarities, but also are consistent with meaningful non-visual semantic interpretations. Second, our *video summary is automatically tagged* as the result of model inference. This is made possible through exploiting the non-visual data distributions associated with the discovered clusters on the training data (see Eqn. (13) and Fig. 2(d)). Below we discuss the details of generating a multi-source video summary.

### 4.1 Key-Clip Extraction and Composition

Suppose we are given a previously unseen surveillance video footage without meta-data tagging/script. The video is pre-processed by segmenting it into a set of  $M$  either overlapping or non-overlapping short clips  $\{\mathbf{x}_i^*\}_{i=1}^M$  with equal duration. Our aim is to first assign cluster membership to each unseen clip using the trained multi-source clustering model, and then select key-clips from the resulting clusters.

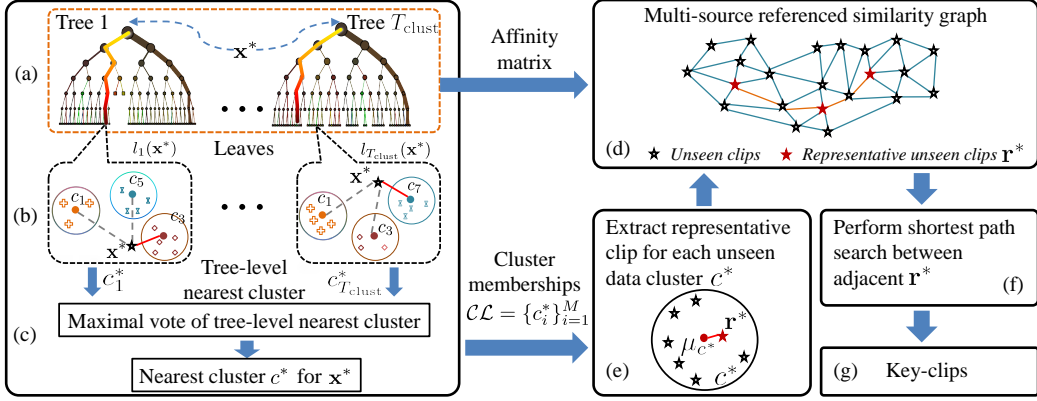


Fig. 4. The pipeline of our multi-source referenced key-clips detection algorithm. (a) Channel a clip  $x^*$  into CC-trees. (b) Search tree-level nearest clusters of  $x^*$ , hollow circle denotes cluster. (c) Predict the final nearest cluster. A red  $\star$  depicts a representative unseen clip.

The chosen key-clips are then chronologically ordered to construct a video summary.

**Clustering unseen video clips** - Inferring cluster memberships of unseen clips is an intricate task. A straightforward method is to assign cluster membership by identifying the nearest cluster  $c^* \in \mathcal{C}$  to a sample  $x^*$ , where  $\mathcal{C}$  represents the set of clusters we discovered in Section 3.3. However, we found this hard cluster assignment strategy susceptible to outliers in  $\mathcal{C}$  and source noise. To mitigate this problem, we consider an alternative approach by utilising the CC-Forest tree structures for soft cluster assignment. This is more robust to either source noise or outliers.

Fig. 4 depicts the soft cluster assignment pipeline. First, we trace the leaf  $l_t(x^*)$  of each tree  $t$  where  $x^*$  falls by channelling  $x^*$  into the tree (Fig. 4(a)). This step is critical as it establishes a connection for  $x^*$  with an appropriate training subset  $\mathbf{X}_{l_t(x^*)}$  using the split functions  $\{h\}_t$  optimised by multi-source data. Here,  $\mathbf{X}_{l_t(x^*)}$  represents the set of training samples associated with  $l_t(x^*)$ . The set is consistent with  $x^*$  both visually and semantically since they encompass identical response w.r.t  $\{h\}_t$ .

Second, we retrieve the cluster membership  $C_t = \{c_i\} \subset \mathcal{C}$  of  $\mathbf{X}_{l_t(x^*)}$ , against which we search for the tree-level nearest cluster  $c_t^*$  for  $x^*$  (Fig. 4(b)) via

$$c_t^* = \operatorname{argmin}_{c \in C_t} \|x^* - \mu_c\|, \quad (14)$$

with  $t$  the tree index, and  $\mu_c$  the centroid of cluster  $c$ , estimated as

$$\mu_c = \frac{1}{|\mathbf{X}_c|} \sum_{x_i \in \mathbf{X}_c} x_i, \quad (15)$$

where  $\mathbf{X}_c$  represents the set of training samples in  $c$ . Performing nearest cluster search within  $C_t$  rather than the whole cluster space  $\mathcal{C}$  brings a key benefit: since the search space is constrained by CC-tree, it is more meaningful and also less noisy than the entire space  $\mathcal{C}$ , leading to more accurate  $c_t^*$  estimation.

Once we obtain all tree-level nearest clusters from all the trees in the forest,  $\{c_t^*\}_{t=1}^{T_{\text{clust}}}$ , the final nearest cluster  $c^*$  is obtained as the one with maximal votes from all the trees (Fig. 4(c))

$$c^* = \max \{c_t^*\}_{t=1}^{T_{\text{clust}}} \quad (16)$$

By repeating the above steps on all unseen clips  $\{x_i^*\}_{i=1}^M$ , we obtain their cluster labels as  $\mathcal{CL} = \{c_i^*\}_{i=1}^M$  (Fig. 4(e)).

**Extracting key-clips** - With the assigned cluster memberships  $\mathcal{CL}$  on all unseen clips, the key-clip of an unseen video data cluster  $c^*$  can be represented by the representative unseen clip  $\mathbf{r}^*$  that is closest to the cluster centroid  $\mu_{c^*}$  (Fig. 4(e)). Concatenating these key-clips chronologically establishes a visual summary. Such a summary, however, is likely to be discontinuous in preserving visual context therefore non-smooth visually due to abrupt changes between adjacent key-clips. To enforce some degrees of smoothness in the visualisation of video summary whilst minimising redundancy, we adopt a shortest path strategy [51] to induce an optimal path between two temporally-adjacent representative  $\mathbf{r}^*$  on a graph  $G$ . This approach produces a visually more coherent video summary whilst discards as much redundancy as possible.

More precisely, we construct a graph  $G = (V, E)$ , where  $V$  and  $E$  indicate the set of unseen video clip vertices and edges (Fig. 4(d)). The weights of edges can be efficiently estimated using Eqn. (11) and (12). Note that graph  $G$  is also multi-source referenced since it is derived from our multi-source CC-Forest model. We then perform shortest path search between temporally-adjacent  $\mathbf{r}^*$  on  $G$  (Fig. 4(f)) and all the samples that lie on the shortest paths compose the final key-clip set  $\mathcal{K}$  (Fig. 4(g)).

## 4.2 Non-Visual Tag Inference

Summarising video with high-level interpretation requires plausible semantic content inference from video data  $x^*$ . We derive a tree-structure aware tag inference algorithm capable of predicting tag types same as training non-visual data, based on the learned CC-Forest and discovered training data clusters. Specifically, we first obtain the tree-level nearest cluster  $c_t^*$  of an unseen sample  $x^*$  using Eqn. (14). Second, the  $p(y_i|c_t^*)$  associated with  $c_t^*$  is utilised as the tree-level non-visual tag estimation for the  $i$ th non-visual data type. To achieve a smooth prediction, we average all  $p(y_i|c = c_t^*)$  obtained from individual trees as

$$p(y_i|x^*) = \frac{1}{T_{\text{clust}}} \sum_{t=1}^{T_{\text{clust}}} p(y_i|c_t^*). \quad (17)$$

The final tag  $\hat{y}_i$  for the  $i$ th non-visual type is obtained as

$$\hat{y}_i = \operatorname{argmax}_{y_i} p(y_i | \mathbf{x}^*). \quad (18)$$

With the above steps, we can estimate all  $m$  non-visual tags  $\hat{y}_i$ s with  $i \in \{1, \dots, m\}$ . The procedure of our tagging algorithm is summarised in Algorithm 1.

---

**Algorithm 1:** Infer non-visual tags of unseen clips.

---

**Input:** An unseen clip  $\mathbf{x}^*$ , a trained CC-Forest, training data clusters  $\mathcal{C}$ ;  
**Output:** Predicted tag  $\hat{y}_i$ ;

- 1 **Initialisation:**
- 2   Compute  $p(y_i | c)$  for each training data cluster (Eqn. (13));
- 3   Compute cluster centroid  $\mu_c$  (Eqn. (15));
- 4 **Non-Visual Tag Inference:**
- 5 **for**  $t \leftarrow 1$  **to**  $T_{\text{clust}}$  **do**
- 6   Trace the leaf  $\ell_t(\mathbf{x}^*)$  where  $\mathbf{x}^*$  falls (Fig. 4(a));
- 7   Retrieve the training samples  $\mathbf{X}_{\ell_t(\mathbf{x}^*)}$  associated with  $\ell_t(\mathbf{x}^*)$ ;
- 8   Obtain the clusters  $C_t = \{c_i\} \subset \mathcal{C}$  of  $\mathbf{X}_{\ell_t(\mathbf{x}^*)}$ ;
- 9   Search the tree-level nearest cluster  $c_t^*$  of  $\mathbf{x}^*$  within  $C_t$  (Eqn. (14));
- 10 **end**
- 11 Estimate tag distribution  $p(y_i | \mathbf{x}^*)$  (Eqn. (17));
- 12 Compute the final tag  $\hat{y}_i$  (Eqn. (18)).

---

Given the extracted key-clips  $\mathcal{K}$  and automatic assignment of non-visual semantic tags (Eqn. (18)), we can now construct a video summary by chronologically concatenating each clip  $\mathbf{x}^* \in \mathcal{K}$  with smooth inter-clip transition, e.g. crossfading, and labelling each clip with their inferred semantic tags.

## 5 EXPERIMENTAL SETTINGS

**Datasets** - We conducted experiments on two datasets collected from publicly accessible webcams that feature an outdoor and an indoor scene respectively: (1) the Times Square Intersection (TISI) dataset, and (2) the Educational Resource Centre (ERCe) dataset<sup>4</sup>. There are a total of 7324 video clips spanning over 14 days in the TISI dataset, whilst a total of 13817 clips were collected across a period of two months in the ERCe dataset. Each clip has a duration of 20 seconds. The details of the datasets and training/deployment partitions are given in Table 1. Example frames are shown in Fig. 5.

The TISI dataset is challenging due to severe inter-object occlusion, complex behaviour patterns, and large illumination variations caused by both natural and artificial light sources at different day time. The ERCe dataset is non-trivial due to a wide range of physical events involved that are characterised by large changes in environmental setup, participants, crowdedness, and intricate activity patterns.

TABLE 1

Details of datasets. FPS = frames per second.

-	Resolution	FPS	# Training Clip	# Deployment Clip
TISI	550 × 960	10	5819	1505
ERCe	480 × 640	5	9387	4430

4. Datasets available: [www.eecs.qmul.ac.uk/%7Exz303/download.html](http://www.eecs.qmul.ac.uk/%7Exz303/download.html)



Fig. 5. Examples of the (a) TISI and (b) ERCE datasets.

**Visual and non-visual sources** - We extracted the following set of visual features for representing visual content in each clip: (a) colour features including RGB and HSV; (b) local texture features based on Local Binary Pattern (LBP) [52]; (c) optical flow; (d) holistic features of the scene based on GIST [53]; and (e) person and vehicle detection [54]<sup>5</sup>.

We collected 10 types of non-visual sources for the TISI dataset: (a) weather data extracted from the WorldWeatherOnline with 9 elements: temperature, weather type, wind speed, wind direction, precipitation, humidity, visibility, pressure, and cloud cover; (b) traffic speed data from the Google Maps with 4 levels of traffic speed: very slow, slow, moderate, and fast. For the ERCE dataset, we collected data from multiple independent on-line sources about the time table of campus events including: No Scheduled Event (No Schd. Event), Cleaning, Career Fair, Gun Forum Control and Gun Violence (Gun Forum), Group Studying, Scholarship Competition (Schlr. Comp.), Accommodative Service (Accom. Service), Student Orientation (Stud. Orient.).

Note that other visual features and non-visual data types can be considered without altering the training and inference methods of our model in that the CC-Forest model is capable of coping with different families of visual features as well as distinct types of non-visual sources.

**Baselines** - To evaluate the proposed method for multi-source video clustering and tag inference, we compared the Visual + Non-Visual + CC-Forest (*VNV-CC-Forest*) model against the following baseline models: (1) *VO-Forest*: a conventional forest [35] trained with visual feature vectors alone, to demonstrate the benefits from using non-visual sources<sup>6</sup>. (2) *VNV-Kmeans*:  $k$ -means using concatenated vectors of visual and non-visual features, to highlight the heteroscedasticity and dimensionality discrepancy problem caused by heterogeneous visual and non-visual data. (3) *VNV-Forest*: a conventional forest [35] trained with concatenated visual and non-visual feature vectors, to compare the effectiveness of CC-Forest that exploits non-visual data as constraints during forest formation. (4) *VNV-AASC*: a state-of-the-art multi-source spectral clustering method [15]

5. No vehicle detection on the ERCE dataset.

6. Evaluating a forest that takes only non-visual inputs is not possible, since non-visual data is not available for previously unseen video footages.

TABLE 2

Compare cluster purity in mean entropy. Lower is better.

Dataset	TISI		ERCe
	traffic speed	weather	event
VO-Forest	0.8675	1.0676	0.0616
VNV-Kmeans	0.9197	1.4994	1.2519
VNV-Forest	0.8611	1.0889	0.0811
VNV-AASC	0.7217	0.7039	0.0691
VT-CC-Forest	0.7275	0.9577	0.0580
VNV-CC-Forest	0.7262	<b>0.6071</b>	<b>0.0024</b>
VPNV10-CC-Forest	<b>0.7190</b>	0.6261	<b>0.0024</b>
VPNV20-CC-Forest	0.7283	0.6497	0.0090

learned by treating each type of visual or non-visual feature as an individual source, to demonstrate the superiority of CC-Forest in handling diverse data representations and correlating multiple sources. (5) *VNV-CC-Forest-hard*: a variant of our model using hard cluster assignment strategy for inferring semantic tags of unseen samples (Section 4.2), to highlight the effectiveness of the proposed tree structure based tag inference algorithm. (6) *VT-CC-Forest*: a variant of our model using only temporal constraint over visual data. In order to show the exact effectiveness of exploiting non-visual data, the weight ratio between visual data and time retains the same as in VNV-CC-Forest with the only difference of discarding non-visual data during model training. (7) *VPNV $\rho$ -CC-Forest*: a variant of our model but with  $\rho\%$  of training samples having arbitrary number of missing non-visual types, to evaluate the robustness of CC-Forest in coping with partial/missing non-visual data.

**Implementation details** - The clustering forest size  $T_{\text{clust}}$  was set to 1000. We observed a slight increase in performance given a larger forest size, which agrees with [16]. The training set  $\mathbf{X}_t$  of the  $t$ th CC-tree was obtained by performing random selection with replacement from the augmented data space (Fig. 3(b)). We set  $m_{\text{try}} = \sqrt{d}$  with  $d$  the data feature dimension (Eqn. (2)). This is typically practiced [35]. We employed linear data separation [16] as the test function for node splitting. We set the same number of clusters across all methods. This cluster number was discovered automatically using the method presented in [50]. For each dataset,  $\sim 75\%$  out of the total data was utilised for model training, and the remaining was reserved for testing. Additional unseen video data was collected from the Time Square Intersection scene on a separate day for video summarisation.

## 6 EVALUATIONS

### 6.1 Multi-Source Video Clustering

To evaluate the effectiveness of different clustering models for multi-source video clustering, we compared the quality of their clusters formed on the training dataset. For determining clustering quality, we quantitatively measured the mean entropy [55] of non-visual distributions  $p(y_i|c)$  (Eqn. (13)) associated with training data clusters to evaluate how coherent video content are partitioned, assuming all methods have access to non-visual data during the entropy computation.



Fig. 6. Qualitative comparison on cluster quality on TISI. A key frame of each video is shown. (X/Y) in brackets: X = the number of clips with sunny weather; Y = the total number of clips in a cluster. The frames inside the red boxes are inconsistent clips in a cluster.

It is evident from Table 2 that our VNV-CC-Forest achieves the best cluster purity on both datasets<sup>7</sup>. Despite that there are gradual degradations in clustering quality when we increase the non-visual data missing proportion, overall the VNV-CC-Forest model copes well with partial/missing non-visual data. With no aid of non-visual tag information, VT-CC-Forest forms much worse clusters. Whilst the superiority of VT-CC-Forest over VO-Forest suggests the effectiveness of temporal constraints with CC-Forest. Inferior performance of VO-Forest to VNV-CC-Forest suggests the importance of learning from auxiliary non-visual sources. Nevertheless, not all methods perform equally well when learning from the same visual and non-visual sources: the  $k$ -means and AASC perform much poorer in comparison to CC-Forest. The results suggest the proposed joint information gain criterion (Eqn. (4)) is more effective in handling heterogeneous data than the conventional clustering models.

For qualitative comparison, we show examples in Fig. 6 using the TISI dataset for detecting ‘sunny’ weather<sup>8</sup>. It is evident that only VNV-CC-Forest is able to provide coherent video grouping. Other methods including VNV-AASC result in a large cluster either leaving out some relevant clips or including many non-relevant ones, with most of them under the influence of strong artificial lighting sources. These non-relevant clips are visually ‘close’ to sunny weather, but semantically not. The VNV-CC-Forest model avoids this mistake by correlating both visual and non-visual sources in an information theoretic sense.

### 6.2 Multi-Source Video Tagging

Generating video synopsis with semantical interpretations requires accurate tag prediction. In this experiment we compared the performance of different methods in inferring semantic tags given unseen clips extracted from long videos. The proposed tagging algorithm (Section 4.2) is used for VO-Forest, VT-CC-Forest, VNV-CC-Forest, VPNV10/20-CC-Forest, whilst nearest neighbour (NN) strategy for the others. For quantitative evaluation, we manually annotated 3 weather conditions (sunny, cloudy and rainy) and 4 traffic speeds on TISI unseen clips, whilst 8 event categories on ERCe unseen clips.

<sup>7</sup>. VNV-CC-Forest-hard shares the same clusters as VNV-CC-Forest.

<sup>8</sup>. The results by variants of CC-Forest are omitted due to space limit.

TABLE 3

Comparison of tagging accuracy on the TISI dataset.

(%)	traffic speed	weather
VO-Forest	27.62	50.65
VNV-Kmeans	37.80	43.14
VNV-Forest	34.95	43.81
VNV-AASC	36.13	44.37
VNV-CC-Forest-hard	32.86	49.59
VT-CC-Forest	35.99	54.47
VNV-CC-Forest	35.77	<b>61.05</b>
VPNV10-CC-Forest	37.99	55.99
VPNV20-CC-Forest	<b>38.05</b>	54.97

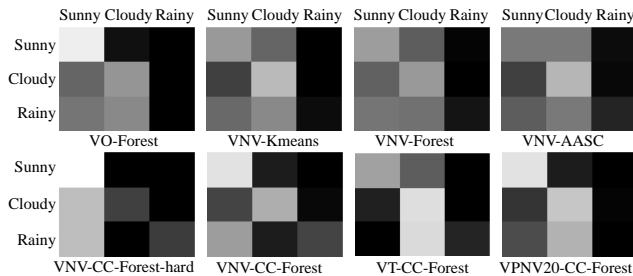


Fig. 7. Weather tagging confusion matrices (TISI dataset).

**Tagging video by weather and traffic conditions** - The experiment was conducted on the TISI outdoor dataset. It is observed that the performance of different methods (Table 3) is largely in line with their performance in data clustering (Section 6.1). The poorest result of tagging traffic conditions is yielded by VO-Forest. This suggests the significance of exploiting non-visual data during model training. It is also seen from Fig. 7 that VNV-CC-Forest not only outperforms other baselines in isolating the sunny weather, but also performs well in distinguishing visually ambiguous cloudy and rainy weathers. In contrast, both VNV-Kmeans and VNV-AASC mistake most of the ‘rainy’ scenes as either ‘sunny’ or ‘cloudy’, as they can be visually similar.

**Tagging video by activity events** - Tagging semantic events was tested using the ERCe dataset. By VO-Forest, poor results (Table 4 and Fig. 8) are obtained especially on Accom. Service, which involves subtle activity patterns, i.e. students visiting particular rooms, suggesting using visual data alone is not sufficient to detect such events. VT-CC-Forest over-fits to ‘Cleaning’ event, therefore performs poorly on ‘Stud. Orient’ event.

Due to the typical high-dimension of visual sources compared to non-visual data, the latter is often overwhelmed by the former in representation. VNV-Kmeans

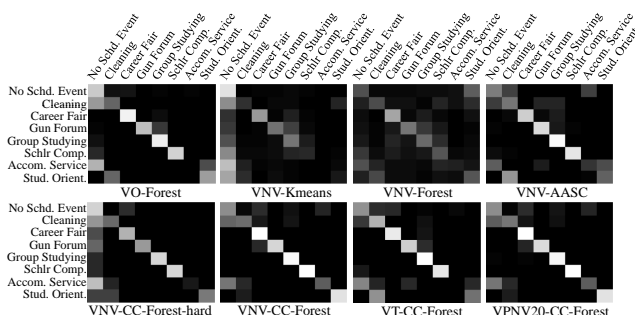
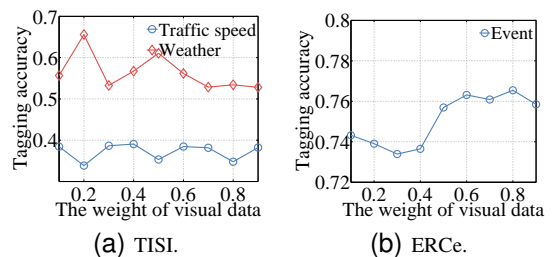


Fig. 8. Event tagging confusion matrices (ERCe dataset).

severely suffers from this problem as its most predictions are biased to No Sched. Event that is more common and frequent visually. This suggests that this distance-based clustering is poor in handling the heteroscedasticity and dimension discrepancy problems in learning heterogeneous data. VNV-AASC attempts to circumvent these problems by seeking for an optimal combination of affinity matrices derived independently from distinct data sources. However this is proved challenging, particularly when each source is inherently noisy and inaccurate. In contrast, the proposed CC-Forest correlates different sources via a joint information gain criterion to effectively alleviate these problems, leading to more robust and accurate tagging performance. Again, VPNV10/20-CC-Forest perform comparably to VNV-CC-Forest, further validating the robustness of CC-Forest in tackling partial/missing non-visual data with the proposed adaptive weighting mechanism (Section 3.2.1).

Interestingly, in some cases, VPNV10/20-CC-Forest models even outperform VNV-CC-Forest slightly. We observe that this can be caused by missing noisy non-visual data, which may lead to better results. Overall, the performance difference is marginal and the results demonstrate that CC-Forest provides stable tagging results across both datasets.

**$\alpha$  sensitivity** - We analyse the relative significance of visual data against non-visual and temporal data by varying its weight  $\alpha_v$  (Eqn. (4)) in CC-Forest during model training. The average tagging accuracy is utilised as performance measure criterion. It is observed from Fig. 9 that setting  $\alpha_v = 0.5$  achieves satisfactory results for both datasets. This observation suggests that visual and non-visual data are almost equally informative. This setting of  $\alpha$  is adopted throughout our experiments.

Fig. 9. The average tagging accuracy against varying visual data weight  $\alpha_v$  in Eqn. (4).

**Further analysis** - The superior performance of VNV-CC-Forest can be better explained by examining more closely the capacity of CC-Forest in uncovering and exploiting the intrinsic correlation among different visual sources and more critically among visual and non-visual sources. This indirect correlation among heterogeneous sources results in well-structured decision trees, subsequently leading to more consistent data clusters and more accurate semantics inference. We show an example here. It is intuitive that vehicle and person counts should correlate in a busy scene like TISI. Our CC-Forest discovered this correlation (see Fig. 10(a)), so the less reliable vehicle detection from distance against a cluttered background, could enjoy a latent support from

TABLE 4  
Comparison of tagging accuracy on the ERCe dataset.

(%)	VO-Forest	VNV-Kmeans	VNV-Forest	VNV-AASC	VNV-CC-Forest-hard	VT-CC-Forest	VNV-CC-Forest	VPNV10-Forest	VPNV20-CC-Forest
No Sched. Event	79.48	<b>87.91</b>	32.47	48.51	81.25	57.43	55.98	47.96	55.57
Cleaning	39.50	19.33	30.25	45.80	41.60	<b>70.17</b>	41.28	46.64	46.22
Career Fair	94.41	59.38	65.46	79.77	70.07	91.45	<b>100.0</b>	<b>100.0</b>	<b>100.0</b>
Gun Forum	74.82	44.30	45.77	84.93	60.48	79.96	83.82	<b>85.29</b>	<b>85.29</b>
Group Studying	92.97	46.25	41.25	96.88	84.22	<b>99.22</b>	97.66	97.66	95.78
Schlr Comp.	82.74	16.71	33.15	89.40	82.88	90.08	99.46	<b>99.73</b>	99.59
Accom. Service	0.00	0.00	13.70	21.15	10.82	0.00	<b>37.26</b>	<b>37.26</b>	37.02
Stud. Orient.	60.94	9.77	33.59	38.87	47.85	43.75	88.09	<b>92.38</b>	88.09
Average	65.61	35.45	36.96	63.16	59.89	66.50	75.69	75.87	<b>75.95</b>

more reliable person detection in regions 5-16 close to the camera view.

Moreover, visual sources also benefit from correlated support from non-visual data through our cross-sources information gain optimisation (Eqn. (4)). An example is the intuitive correlation between traffic speed and visual appearance, e.g. slow traffic speed often corresponds to crowded scenarios with a large quantity of pedestrians and vehicles whilst fast traffic speed to sparse people and cars. Such cross-source correlation can be captured by our CC-Forest, as observed in Fig. 10(b) that the vehicle detection responses over road area present a stronger interaction with traffic speed data than those on walk path where vehicles should not appear. In other words, vehicle detection features of road area are preferred over those on walk path in node splitting due to larger induced joint information gain (Eqn. (4)), which is clearly desired. This discovered correlation is further exploited by CC-Forest during the node splitting optimisation process and thus facilitates the separation of different crowdedness levels of visual data. This leads to better clusters and eventually benefits video summarisation.

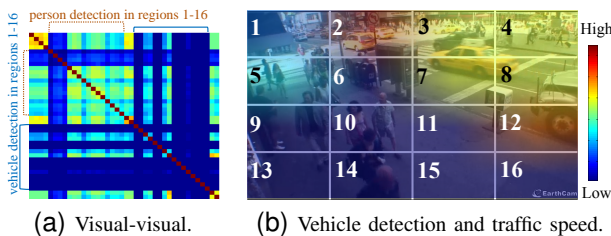


Fig. 10. The discovered multi-source correlation on TISI.

### 6.3 Multi-Source Video Summarisation

In this experiment, we follow the method described in Section 4, and show that the learned model CC-Forest can be easily extended to produce compact yet meaningful video summary of previously unseen video footage, e.g. from the Time Square Intersection scene, with automatically generated semantic tags. Despite captured from the same scene as the TISI dataset, this unseen video is challenging in that it contains a number of events not seen before (e.g. scaffolding event), with very different weather and traffic conditions. It is interesting to examine how well the multi-source model could generalise for drawing meaningful summarisation given such unexpected disparities.

#### 6.3.1 A Quantitative Evaluation on Synopsis Quality

Measuring the quality of synopsis quantitatively is non-trivial since there is no formal definition in the literature. In

this study, we employ a *coverage* metric – an ideal synopsis should cover as many events of interest as possible<sup>9</sup>. More precisely, given a video synopsis  $\mathcal{V}$ , its coverage is defined as  $\tilde{c} = \frac{N_{\text{covered}}}{N_{\text{all}}} \left( \frac{\max_i |\mathcal{V}_i|}{|\mathcal{V}|} \right)$ , where  $N_{\text{covered}}$  and  $N_{\text{all}}$  represent the number of covered and all events of interest, respectively. The  $|\mathcal{V}|$  is the length of the current synopsis, whilst  $\max_i |\mathcal{V}_i|$  represents the maximum length of all comparative synopses. The term  $\left( \frac{\max_i |\mathcal{V}_i|}{|\mathcal{V}|} \right)$  thus penalises a synopsis with longer length. Higher coverage is better, implying lower redundancy.

In order to generate unbiased ground truth of event of interest, we asked 10 annotators to watch the previously unseen video carefully and label each video clip with arbitrary event tags. Although these event tags were produced independently in a somewhat subjective manner, the repetition of similar tagging among different annotators is high, e.g. most annotators labelled ‘unloading scaffolding tubes’, ‘policemen on-duty’, as events of their interest. Thus, we formed the ground truth with events that were agreed by over 50% of the annotators. The final ground truth consists of 12 events (Fig. 11).

Given the ground truth, we compared the quality of synopsis generated using the proposed multi-source CC-Forest with the baselines: (1) Uniform-Sampling: a straightforward way of summarising video by uniformly sampling video clips over time, assuming key events are distributed evenly [32], [11]. (2) Sufficient-Change: a classical summarisation strategy generic to video category [31], [56], [32]. The idea is to select the clip significantly different from the previous key clip e.g. using threshold based strategy and thus the extracted key clips may be of great diversity and complete. The threshold can be estimated based on the number of key clips. For the distance metric, we adopt L1-norm and L2-norm to measure pairwise similarity between clips in our experiment. (3) VO-Forest: the conventional Forest [35] that exploits visual features alone. For VO-Forest and CC-Forest, we applied the summarisation pipeline described in Section 4 for synopsis composition. We generated the video summary by the remaining methods via setting a duration similar to the synopsis by CC-Forest. Note that non-visual information are not available during the summarisation stage. Hence, for clustering based models, the quality of a synopsis essentially ties to the purity and coherency of video clusters discovered using different methods.

The results are shown in Fig. 11 and Table 5. It is evident

<sup>9</sup> The event of interest is analogous to important objects/regions in [11].

TABLE 5  
Quantitative comparison of synopsis.

Method	Length (clips)	Event number	Coverage
Uniform-Sampling	28	3	25.9%
Sufficient-Change(L1)	29	2	16.7%
Sufficient-Change(L2)	29	4	33.3%
VO-Forest	21	3	34.5%
VNV-CC-Forest(Ours)	28	7	60.4%

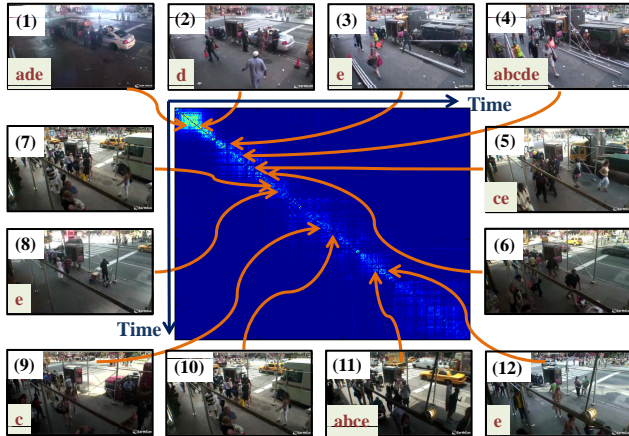


Fig. 11. The multi-source affinity matrix constructed by our model, along with key frames corresponding to ground truth events of interest: (1) policemen on-duty, (2) blocking pathway, (3) workers unloading scaffolding tubes, (4)-(6) different stages of scaffolding, (7)(9)(10) van parking aside, (8) parcel delivery, (11)(12) loitering events. The event covered by some particular method is indicated on the left-bottom corner of key frame with their ID defined as: (a) Uniform-Sampling; (b) Sufficient-Change(L1); (c) Sufficient-Change(L2); (d) VO-Forest; (e) VNV-CC-Forest.

that the CC-Forest model achieves higher event coverage than the baselines. This is in large due to the CC-Forest’s ability for latent data structure discovery (Section 6.1). To reveal concrete reasons on the summarising performance difference, for the same unseen samples  $x^*$  with event of interest, e.g. parcel delivery, we compared the assigned clusters:  $c_{vnn}^*$  by our model and  $c_{vo}^*$  by VO-Forest. It is found that samples in  $c_{vnn}^*$  are visually consistent each other and the majority share some similarity with  $x^*$ , e.g. someone standing at the edge of pathway; whilst cluster  $c_{vo}^*$  is much larger with no obvious visual commonality over its cluster members. Uniform-Sampling performs poorly since the assumption of uniform event distribution is often invalid. Significant-Change is inferior to our model since the visual data distance/similarity measure can be inaccurate and less meaningful due to the challenging semantic gap problem.

### 6.3.2 A User Study on Synopsis Quality

We conducted a user study to examine if the non-visual tags inferred using the CC-Forest model could complement the unilateral perspective offered by pure visual summary alone. We showed two video summaries to 10 volunteers: (i) a pure visual summary, and (ii) the same summary but enriched with semantic tags inferred using the proposed multi-source model<sup>10</sup>. The tagged summary is shown in

10. The inferred non-visual tags include weather, traffic conditions, and typicality. The typicality tag, i.e. *usual* and *interesting*, of each clip, is computed based on the size of their assigned clusters (Fig. 4(c)). Clips assigned to the top 20% smallest clusters are treated as ‘interesting’.

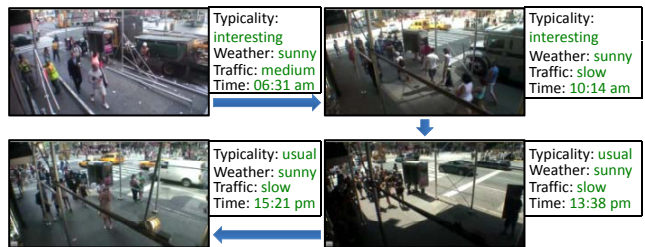


Fig. 12. A storyboard version of our video synopsis enriched with non-visual tags.

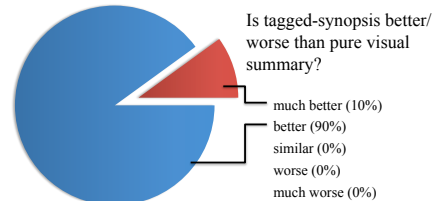


Fig. 13. User study: tagged *versus* pure-visual summary.

Fig. 12. Each volunteer was asked to compare and rate the two summaries based on their preference. It is worth pointing out that passing the user test is challenging because providing additional non-visual tags to synopsis is not necessarily better than none. Tags that correlate poorly with visual context could even jeopardise user experience.

It is evident from Fig. 13 that visual summary augmented with non-visual tags was well accepted by all participants over the conventional visual-only synopsis. A follow-up survey with the volunteers reveals several interesting reasons of their selection. Many volunteers found that the inferred non-visual tags were valuable in providing auxiliary context to achieve better global situational awareness. In particular, the tags helped them to ‘connect the dots’ and making sense of the unseen (and likely unfamiliar) video footages. Some other volunteers credited the additional non-visual tags in focusing their attention on particular events, and helping them in spotting ‘outliers’ of interest.

This user study provides an independent means to analyse and validate the usefulness of visual summarisation with auto-tag inference of previously unseen video footages without a priori semantics or meta-data, mostly typical of surveillance videos. It also shows the effectiveness of the proposed model for mapping multi-source non-visual information to unstructured and unseen video data in automatic tagging and summarisation of the videos.

### 6.4 Computational Costs and Model Complexity

We examined the computational costs for training the proposed CC-Forest, in comparison to the conventional forests. Time is measured on a Windows PC machine with a dual-core CPU @ 2.66 GHz, 4.0GB RAM, with C++ implementation. Only one core is utilised for training each forest. We recorded the model training time under the same experimental setting as stated in Section 5. It is observed from Table 6 that the training cost of a CC-Forest model is significantly lower than that of learning conventional forests. In particular, VNV-CC-Forest records a reduced training time by 14.4% and 17.1% on TISI, and 64.1%

and 64.4% on ERCe, when compared with VO-Forest and VNV-Forest, respectively. We observed similar trend on the model inference time.

The lower computational cost of CC-Forest is owing to its shallow and balanced trees, thanks to the additional non-visual and temporal constraints during tree optimisation. To make this concrete, we showed in Table 6 the averaged tree fan-in  $\Phi^* = \frac{1}{T_{\text{clust}}} \sum_t^{T_{\text{clust}}} \Phi(t)$  of different forest models. A forest with shallow and balanced trees tend to have a small  $\Phi^*$  (see Section 3.2.3 for a discussion on tree fan-in). In addition, we also profiled the length of path (from root to leaf node) traversed by training samples. A shallow and balanced tree tends to have shorter path length. The distributions depicted in Fig. 14 suggest that CC-Forest has a shallower and more balanced tree topology than that of conventional forests. It is worth pointing out that despite the shallower structure, CC-Forest outperforms other models in our clustering and tagging experiments.

TABLE 6  
Forest model training complexity. Lower is better.

Dataset	TISI		ERCe	
	Training (sec.)	$\Phi^*$	Training (sec.)	$\Phi^*$
-				
VO-Forest	10306	109392	21831	359247
VNV-Forest	10646	108865	22015	359364
VNV-CC-Forest	<b>8823</b>	<b>91316</b>	<b>7845</b>	<b>137620</b>

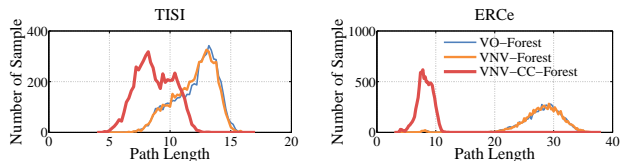


Fig. 14. Comparing tree path length statistics. The same legend is used for both charts.

## 7 CONCLUSION AND FUTURE WORK

We have presented a novel unsupervised multi-source learning model for video summarisation. Specifically, we introduced a joint information gain function for discovering and exploiting latent correlations among independent heterogeneous data sources. The function naturally copes with diverse types of data with different representations, distributions, and dimensions. Importantly, our model is capable of tolerating partial and missing non-visual data, lending it well for automatic semantic tag inference on previously unseen video footages and for video summarisation. Furthermore, the proposed joint constraint optimisation encourages more compact decision trees, leading to more efficient model training and semantic tag inference. Comparative experiments have demonstrated the advantages of the proposed multi-source video clustering model over existing visual-only models, for both discovering latent video clusters and inferring non-visual semantic tags on previously unseen video footages. A comprehensive user study was carried out to validate independently the effectiveness of deploying the proposed model for generating contextually-rich and semantically-meaningful video synopsis.

The proposed model is not limited to surveillance-type videos but can be generalised to other types of unstructured

and un-tagged consumer videos or egocentric videos, if 3D camera motion-invariant features or egocentric features [11] are adopted. For future work, we will consider generalising/transferring a learned model to new scenes that are significantly different from the training environments. This can be partly addressed by utilising intermediate data representations such as attributes.

## REFERENCES

- [1] T. M. Hospedales, J. Li, S. Gong, and T. Xiang, "Identifying rare and subtle behaviors: a weakly supervised joint topic model," *Pattern Analysis and Machine Intelligence, IEEE Transactions on*, pp. 2451–2464, 2011.
- [2] X. Wang, X. Ma, and W. E. L. Grimson, "Unsupervised activity perception in crowded and complicated scenes using hierarchical bayesian models," *Pattern Analysis and Machine Intelligence, IEEE Transactions on*, pp. 539–555, 2009.
- [3] S. Wu, B. E. Moore, and M. Shah, "Chaotic invariants of lagrangian particle trajectories for anomaly detection in crowded scenes," in *IEEE Conference on Computer Vision and Pattern Recognition*, 2010, pp. 2054–2060.
- [4] C. C. Loy, T. Xiang, and S. Gong, "Incremental activity modeling in multiple disjoint cameras," *Pattern Analysis and Machine Intelligence, IEEE Transactions on*, pp. 1799–1813, 2012.
- [5] L. Kratz and K. Nishino, "Going with the flow: pedestrian efficiency in crowded scenes," in *European Conference on Computer Vision*, 2012.
- [6] A. B. Chan and N. Vasconcelos, "Modeling, clustering, and segmenting video with mixtures of dynamic textures," *Pattern Analysis and Machine Intelligence, IEEE Transactions on*, pp. 909–926, 2008.
- [7] W. Li, V. Mahadevan, and N. Vasconcelos, "Anomaly detection and localization in crowded scenes," *IEEE Transactions on Pattern Analysis and Machine Intelligence*, 2013.
- [8] H. Kang, X. Chen, Y. Matsushita, and X. Tang, "Space-time video montage," in *IEEE Conference on Computer Vision and Pattern Recognition*, 2006.
- [9] Y. Pritch, A. Rav-Acha, and S. Peleg, "Nonchronological video synopsis and indexing," *IEEE Transactions on Pattern Analysis and Machine Intelligence*, pp. 1971–1984, 2008.
- [10] S. Feng, Z. Lei, D. Yi, and S. Z. Li, "Online content-aware video condensation," in *IEEE Conference on Computer Vision and Pattern Recognition*, 2012.
- [11] Y. J. Lee, J. Ghosh, and K. Grauman, "Discovering important people and objects for egocentric video summarization," in *IEEE Conference on Computer Vision and Pattern Recognition*, 2012.
- [12] Z. Lu and K. Grauman, "Story-driven summarization for egocentric video," in *IEEE Conference on Computer Vision and Pattern Recognition*, 2013.
- [13] S. Gong, C. C. Loy, and T. Xiang, "Security and surveillance," in *Visual Analysis of Humans*. Springer, 2011, pp. 455–472.
- [14] R. Duin and M. Loog, "Linear dimensionality reduction via a heteroscedastic extension of lda: the chernoff criterion," *IEEE Transactions on Pattern Analysis and Machine Intelligence*, pp. 732–739, 2004.
- [15] H.-C. Huang, Y.-Y. Chuang, and C.-S. Chen, "Affinity aggregation for spectral clustering," in *IEEE Conference on Computer Vision and Pattern Recognition*, 2012.
- [16] A. Criminisi and J. Shotton, "Decision forests: A unified framework," *Foundations and Trends in Computer Graphics and Vision*, pp. 81–227, 2012.
- [17] X. Cai, F. Nie, H. Huang, and F. Kamangar, "Heterogeneous image feature integration via multi-modal spectral clustering," in *IEEE Conference on Computer Vision and Pattern Recognition*, 2011.
- [18] J. Heer and E. H. Chi, "Identification of web user traffic composition using multi-modal clustering and information scent," in *Proc. of the Workshop on Web Mining, SIAM Conference on Data Mining*, 2001, pp. 51–58.
- [19] I. Karydis, A. Nanopoulos, H.-H. Gabriel, and M. Spiliopoulou, "Tag-aware spectral clustering of music items," in *ISMIR*, 2009, pp. 159–164.
- [20] D.-Q. Zhang, C.-Y. Lin, S.-F. Chang, and J. R. Smith, "Semantic video clustering across sources using bipartite spectral clustering," in *IEEE International Conference on Multimedia and Expo*, 2004.

- [21] Y. Fu, T. Hospedales, T. Xiang, and S. Gong, "Learning multi-modal latent attributes," *Pattern Analysis and Machine Intelligence, IEEE Transactions on*, 2013.
- [22] C. Taskiran, Z. Pizlo, A. Amir, D. Ponceleon, and E. Delp, "Automated video program summarization using speech transcripts," *Multimedia, IEEE Transactions on*, vol. 8, pp. 775–791, 2006.
- [23] Y. Gong, "Summarizing audiovisual contents of a video program," *EURASIP Journal on Advances in Signal Processing*, pp. 160–169, 2003.
- [24] V. Khalidov, F. Forbes, and R. Horaud, "Conjugate mixture models for clustering multimodal data," *Neural Computation*, vol. 23, pp. 517–557, 2011.
- [25] Z. Wang, M. Zhao, Y. Song, S. Kumar, and B. Li, "Youtubecat: Learning to categorize wild web videos," in *IEEE Conference on Computer Vision and Pattern Recognition*, 2010.
- [26] G. Toderici, H. Aradhye, M. Pasca, L. Sbaiz, and J. Yagnik, "Finding meaning on youtube: Tag recommendation and category discovery," in *IEEE Conference on Computer Vision and Pattern Recognition*, 2010.
- [27] M. Wang, R. Hong, G. Li, Z.-J. Zha, S. Yan, and T.-S. Chua, "Event driven web video summarization by tag localization and key-shot identification," *IEEE Transactions on Multimedia*, pp. 975–985, 2012.
- [28] A. Strehl and J. Ghosh, "Cluster ensembles—a knowledge reuse framework for combining multiple partitions," *The Journal of Machine Learning Research*, vol. 3, pp. 583–617, 2003.
- [29] A. Topchy, A. K. Jain, and W. Punch, "Clustering ensembles: Models of consensus and weak partitions," *Pattern Analysis and Machine Intelligence, IEEE Transactions on*, vol. 27, no. 12, pp. 1866–1881, 2005.
- [30] W. Wolf, "Keyframe selection by motion analysis," in *IEEE International Conference on Acoustics, Speech, and Signal Processing*, 1996.
- [31] H. Zhang, J. Wu, D. Zhong, and S. W. Smoliar, "An integrated system for content-based video retrieval and browsing," *Pattern Recognition*, 1997.
- [32] B. T. Truong and S. Venkatesh, "Video abstraction: A systematic review and classification," *ACM Transactions on Multimedia Computing, Communications, and Applications*, 2007.
- [33] A. G. Money and H. Agius, "Video summarisation: A conceptual framework and survey of the state of the art," *Journal of Visual Communication and Image Representation*, pp. 121–143, 2008.
- [34] Y. Pritch, A. Rav-Acha, A. Gutman, and S. Peleg, "Webcam synopsis: Peeking around the world," in *The IEEE International Conference on Computer Vision*, 2007.
- [35] L. Breiman, "Random forests," *Machine Learning*, 2001.
- [36] J. Shotton, A. Fitzgibbon, M. Cook, T. Sharp, M. Finocchio, R. Moore, A. Kipman, and A. Blake, "Real-time human pose recognition in parts from single depth images," in *IEEE Conference on Computer Vision and Pattern Recognition*, 2011.
- [37] J. Gall, A. Yao, N. Razavi, L. J. V. Gool, and V. S. Lempitsky, "Hough forests for object detection, tracking, and action recognition," *IEEE Transactions on Pattern Analysis and Machine Intelligence*, pp. 2188–2202, 2011.
- [38] S. Schuster, C. Leistner, P. Wohlhart, P. M. Roth, and H. Bischof, "Alternating regression forests for object detection and pose estimation," in *IEEE International Conference on Computer Vision*, 2013.
- [39] A. Bosch, A. Zisserman, and X. Munoz, "Image classification using random forests and ferns," in *IEEE International Conference on Computer Vision*, 2007.
- [40] R. Caruana, N. Karampatziakis, and A. Yessenalina, "An empirical evaluation of supervised learning in high dimensions," in *International conference on Machine learning*, 2008.
- [41] B. Liu, Y. Xia, and P. S. Yu, "Clustering through decision tree construction," in *Conference on Information and Knowledge Management*, 2000.
- [42] T. Shi and S. Horvath, "Unsupervised learning with random forest predictors," *Journal of Computational and Graphical Statistics*, pp. 118–138, 2006.
- [43] F. Perbet, B. Stenger, and A. Maki, "Random forest clustering and application to video segmentation," in *British Machine Vision Conference*, 2009.
- [44] F. Moosmann, E. Nowak, and F. Jurie, "Randomized clustering forests for image classification," *IEEE Transactions on Pattern Analysis and Machine Intelligence*, pp. 1632–1646, 2008.
- [45] X. Zhu, C. C. Loy, and S. Gong, "Constructing robust affinity graphs for spectral clustering," in *Proceedings of the 27th IEEE Conference on Computer Vision and Pattern Recognition*, Jun. 2014, pp. 1450–1457.
- [46] —, "Constrained clustering with imperfect oracles," *Special Issue on Learning in Non-(geo)metric Spaces, IEEE Transactions on Neural Networks and Learning Systems*, 2015.
- [47] S. Schuster, P. Wohlhart, C. Leistner, A. Saffari, P. M. Roth, and H. Bischof, "Alternating decision forests," in *IEEE Conference on Computer Vision and Pattern Recognition*, 2013.
- [48] L. Breiman, J. Friedman, C. Stone, and R. Olshen, *Classification and regression trees*. Chapman & Hall/CRC, 1984.
- [49] J. K. Martin, "An exact probability metric for decision tree splitting and stopping," *Machine Learning*, pp. 257–291, 1997.
- [50] L. Zelnik-manor and P. Perona, "Self-tuning spectral clustering," in *Advances in Neural Information Processing Systems*, 2004.
- [51] S. Boccaletti, V. Latora, Y. Moreno, M. Chavez, and D.-U. Hwang, "Complex networks: Structure and dynamics," *Physics reports*, pp. 175–308, 2006.
- [52] T. Ojala, M. Pietikainen, and T. Maenpaa, "Multiresolution gray-scale and rotation invariant texture classification with local binary patterns," *IEEE Transactions on Pattern Analysis and Machine Intelligence*, pp. 971–987, 2002.
- [53] A. Oliva and A. Torralba, "Modeling the shape of the scene: A holistic representation of the spatial envelope," *International Journal of Computer Vision*, vol. 42, pp. 145–175, 2001.
- [54] P. F. Felzenszwalb, R. B. Girshick, D. A. McAllester, and D. Ramanan, "Object detection with discriminatively trained part-based models," *IEEE Transactions on Pattern Analysis and Machine Intelligence*, pp. 1627–1645, 2010.
- [55] Y. Zhao and G. Karypis, "Empirical and theoretical comparisons of selected criterion functions for document clustering," *Machine Learning*, pp. 311–331, 2004.
- [56] C. Kim and J.-N. Hwang, "Object-based video abstraction for video surveillance systems," *Circuits and Systems for Video Technology, IEEE Transactions on*, vol. 12, pp. 1128–1138, 2002.